

## Randomized low-rank decompositions of nuclear three-body interactions

A. Tichai <sup>1,2,3,\*</sup> P. Arthuis <sup>1,2,4,†</sup> K. Hebeler <sup>1,2,3</sup> M. Heinz <sup>1,2,3,‡</sup> J. Hoppe,<sup>1,2</sup>  
T. Miyagi,<sup>1,2,3,§</sup> A. Schwenk <sup>1,2,3</sup> and L. Zurek <sup>1,2,||</sup>

<sup>1</sup>*Technische Universität Darmstadt, Department of Physics, 64289 Darmstadt, Germany*

<sup>2</sup>*ExtreMe Matter Institute EMMI, GSI Helmholtzzentrum für Schwerionenforschung GmbH, 64291 Darmstadt, Germany*

<sup>3</sup>*Max-Planck-Institut für Kernphysik, Saupfercheckweg 1, 69117 Heidelberg, Germany*

<sup>4</sup>*Helmholtz Forschungsakademie Hessen für FAIR (HFHF), GSI Helmholtzzentrum für Schwerionenforschung GmbH, 64291 Darmstadt, Germany*



(Received 11 August 2023; revised 12 December 2023; accepted 26 November 2024; published 31 December 2024)

First-principles simulations of many-fermion systems are commonly limited by the computational requirements of processing large data objects. As a remedy, we propose the use of low-rank approximations of three-body interactions, which are the dominant such limitation in nuclear physics. We introduce a randomized decomposition technique to handle the excessively large matrix dimensions and study the sensitivity of low-rank properties to interaction details. The developed low-rank three-nucleon interactions are benchmarked in *ab initio* simulations of few- and many-body systems. Exploiting low-rank properties provides a promising route to extend the microscopic description of atomic nuclei to large systems where storage requirements exceed the computational capacities of the most advanced high-performance computing facilities.

DOI: [10.1103/PhysRevResearch.6.043331](https://doi.org/10.1103/PhysRevResearch.6.043331)

### I. INTRODUCTION

What is the most efficient way to formulate and solve the quantum many-body problem? This question lies at the heart of many-body theory and impacts areas ranging from atomic physics, condensed matter physics, and quantum chemistry. In nuclear physics, the *ab initio* description of many-body systems has witnessed remarkable progress (see Refs. [1–3]) such that nowadays up to 100 interacting particles and beyond can be targeted in first-principles simulations [4–9]. This great success is due to (i) the development of high-precision nuclear interactions based on chiral effective field theory [3,10–13], and (ii) the use of many-body expansion methods [2]. Basis expansions are widespread in many-body theory, the most common being many-body perturbation theory (MBPT) [14–17], self-consistent Green’s function theory [18–21], coupled-cluster theory [9,22–24], and the in-medium similarity renormalization group (IMSRG) approach [25–28].

All these many-body frameworks have the great benefit of polynomial computational scaling with system size, thus circumventing the computational limitations of variational frameworks such as large-scale diagonalizations from configuration interaction approaches [29] or real-space methods such as quantum Monte Carlo [30].

The fundamental input of basis expansion methods are matrix elements of second-quantized many-body operators and their computational complexity is directly linked to the dimensions of the data arrays that store the matrix elements. Memory requirements quickly become prohibitive when the size of the single-particle basis is increased, e.g., in large systems and/or when symmetries of many-body operators are spontaneously broken [24,31–35]. In particular the handling of three-body operators poses a significant computational challenge. Such higher-mode tensors naturally emerge in the description of nuclear systems and cold atoms (see Refs. [1,36]) or as operators in high-precision calculations [23,28]. Therefore, the treatment of prohibitively large data objects is a universal problem in quantum many-body theory.

In other areas of quantum many-body research it has been recognized for a long time that the complexity of the many-body problem can be tamed by optimizing the representation of the underlying data objects by performing a so-called tensor decomposition, i.e., a rewriting of complex high-dimensional objects as a sum/product of objects with lower dimension [37]. Factorizations are at the heart of tensor-network theories such as the density matrix renormalization group that fundamentally build upon a factorized wave-function ansatz (see Refs. [38–40]) and have been successfully applied in nuclear structure calculations [41–45]. In quantum chemistry, correlation expansions have been revisited in the context of factorized wave-function amplitudes (see Refs. [46–50])

\*Contact author: [alexander.tichai@physik.tu-darmstadt.de](mailto:alexander.tichai@physik.tu-darmstadt.de)

†Present address: Université Paris-Saclay, CNRS/IN2P3, IJCLab, 91405 Orsay, France.

‡Present address: National Center for Computational Sciences, Oak Ridge National Laboratory, Oak Ridge, TN 37830, USA.

§Present address: Center for Computational Sciences, University of Tsukuba, 1-1-1 Tennodai, Tsukuba 305-8577, Japan.

||Present address: Université Paris-Saclay, CEA, Laboratoire Matière en Conditions Extrêmes, 91680 Bruyères-le-Châtel, France.

*Published by the American Physical Society under the terms of the Creative Commons Attribution 4.0 International license. Further distribution of this work must maintain attribution to the author(s) and the published article’s title, journal citation, and DOI. Open access publication funded by Max Planck Society.*

and tensor-decomposed electron-repulsion integrals have been used in electronic-structure calculations [51–53]. While the design of factorized many-body frameworks poses a significant formal challenge, it provides a long-term perspective to problems in many-body theory.

In nuclear physics it was shown that modern nucleon-nucleon (NN) interactions admit for excellent low-rank approximations by employing a singular-value decomposition (SVD) on the momentum-space matrix elements [54,55]. Such low-rank interactions provide an accurate description of nuclear observables in various applications ranging from two-nucleon phase shifts to infinite nuclear matter calculations and ground-state observables in medium-mass nuclei [54]. Moreover, the two-body (Lippmann-Schwinger) scattering equations were recently reformulated such that they can be solved in terms of the decomposition factors themselves without reconstructing the original matrix [56]. In a complementary way, more complex tensor decompositions have been explored to factorize nuclear many-body states [57,58], and random embeddings of nuclear two-body operators have been used to sample perturbative estimates of the correlation energies of closed-shell nuclei [59].

In this work, we explore a scalable randomized linear-algebra solver that overcomes the limitations of traditional decomposition algorithms in terms of matrix dimension. Using this method, low-rank approximations of three-nucleon (3N) forces are derived and benchmarked in few- and many-body applications. Our results thus provide alternative, efficient storage formats of many-body operators and algorithms to obtain them. While this paper focuses on nuclei, the developments are discipline agnostic and can be applied in other domains of many-body research.

## II. RANDOMIZED MATRIX DECOMPOSITIONS

In the following we employ the singular value decomposition (SVD) of the 3N potential (with a dense matrix representation  $V_{3N} \in \mathbb{R}^{N \times N}$  in a basis of size  $N$ )

$$V_{3N} = L \Sigma R^T, \tag{1}$$

where  $L$  ( $R$ ) denotes the unitary left (right) matrix of singular vectors and  $\Sigma$  is a diagonal matrix containing the non-negative singular values  $s_i$  ordered in decreasing size.

The conventional factorization of large matrices is a computationally intensive task. In this work we lower the computational cost of the decomposition by introducing a probabilistic component to the algorithm as proposed by Halko *et al.* (see Ref. [60]). The corresponding randomized SVD (rSVD) algorithm allows one to target the largest singular values much more efficiently.

A schematic representation of the rSVD algorithm is displayed in Fig. 1. In the first step a random projection matrix  $P \in \mathbb{R}^{N \times l}$  is applied to the initial matrix  $V$  yielding a matrix  $Z = VP$  of much smaller size than  $V$ , in particular for low-rank matrices with  $l \ll N$ . Subsequently, an orthonormal basis of  $Z$  is obtained by performing a QR decomposition  $Z = QX$  (step 1). The initial matrix  $V$  is then projected to a smaller space using the low-rank basis  $Q$  yielding  $Y = Q^T V$ . Performing a thin SVD of the projected matrix yields  $Y = L_Y \Sigma R^T$  (step 2). The left SVD component  $L$  of the full

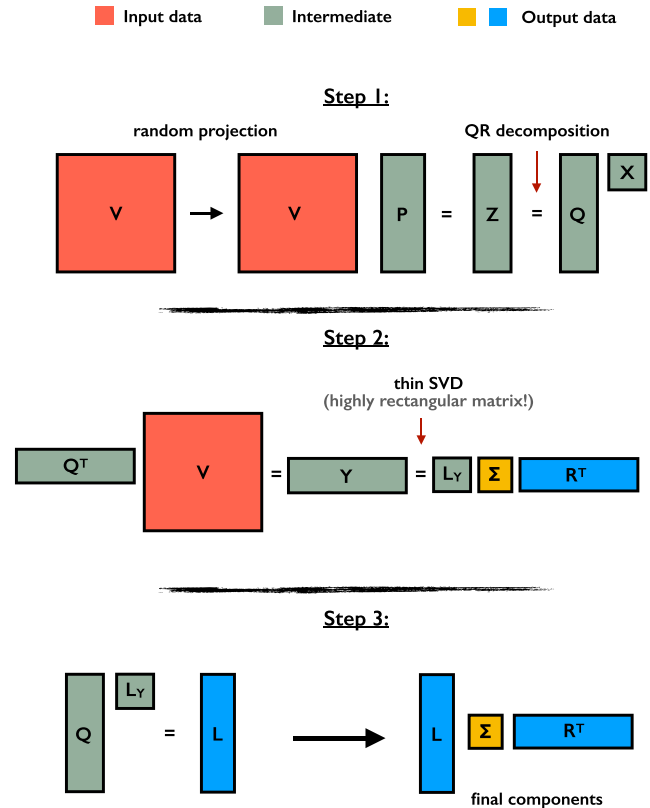


FIG. 1. Algorithmic steps in the calculation of a randomized SVD: (1) random projection and QR decomposition, (2) thin SVD of the projected interaction, (3) final evaluation of the left singular vectors.

decomposition is obtained by final left multiplication with  $Q$ , i.e.,  $L = QL_Y$  (step 3).

In practice the number  $l$  is chosen slightly larger than the desired rank  $R_{\text{SVD}}$ . The difference  $p = l - R_{\text{SVD}}$  is termed oversampling parameter and is introduced to stabilize the computation and lower the sensitivity to the initial random sample. In our applications a value of  $p = 5$  is chosen. The random character only enters through the choice of the initial projection operator  $P$  and only a single run is performed in practice. While the repeated evaluation of the rSVD gives slightly different singular spectra, we validated our findings against an exact SVD for small matrices and found the random error to be negligible. Our rSVD implementation is based on the EIGEN library [61] such that all decompositions can be performed efficiently on a single compute node in a few hours. A numerical implementation will be made publicly available in the future.

Once a decomposition has been obtained, the computational gain of the decomposition is quantified in terms of the compression ratio

$$C_{R_{\text{SVD}}}^N \equiv \frac{N^2}{2NR_{\text{SVD}} + R_{\text{SVD}}}, \tag{2}$$

where  $N$  denotes the matrix dimension and  $R_{\text{SVD}}$  the SVD-rank of the decomposition, i.e., the number of singular values kept. The ratio  $C_{R_{\text{SVD}}}^N$  quantifies the memory savings of a rank- $R_{\text{SVD}}$  approximation over its original full-rank starting

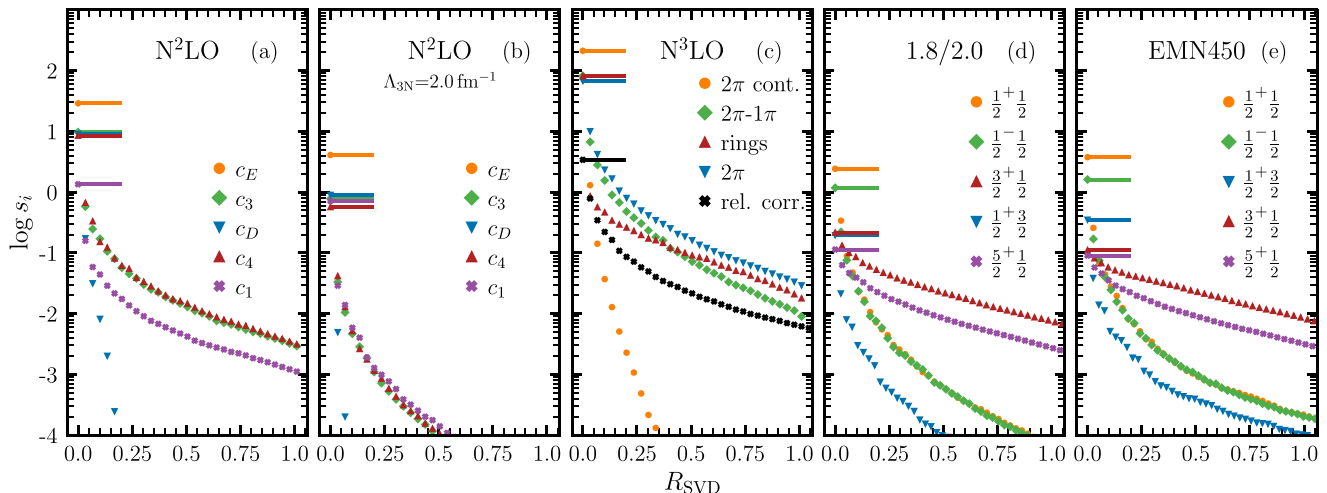


FIG. 2. Logarithm of singular values as a function of truncation rank for different chiral 3N matrix elements: (a) unregularized N<sup>2</sup>LO operator topologies for the triton channel with all LECs set to one; (b) same as (a) but with a regulator of  $\Lambda_{3N} = 2.0 \text{ fm}^{-1}$ ; (c) unregularized N<sup>3</sup>LO topologies again with LECs set to one; and different partial-wave channels of (d) the “1.8/2.0” interaction and (e) the “EMN450” interaction (both including regulators). The leading singular value is indicated by a horizontal line. The legends are ordered according to the size of the largest singular value.

point of a square matrix with linear dimension  $N$ . Since in the following we compare decompositions between matrices of different dimensions, it is useful to introduce the relative SVD-rank  $R_{\text{SVD}}^{\%} \equiv 100 \cdot R_{\text{SVD}}/N$ . This is closely related to the compression ratio such that  $R_{\text{SVD}}^{\%} = 1.0$  corresponds to  $C \approx 100$  and  $R_{\text{SVD}}^{\%} = 0.1$  to  $C \approx 1000$ .

### III. LOW-RANK INTERACTIONS

In practice the rSVD is applied to the partial-wave-decomposed momentum-space matrix elements of 3N interactions

$$\langle pq; \alpha | V_{3N} | p'q'; \alpha' \rangle, \quad (3)$$

where  $p, q$  ( $p', q'$ ) denote the three-body bra (ket) Jacobi momenta and the collective index  $\alpha = \{[(LS)J](ls)j\}$   $\mathcal{J}M_{\mathcal{J}}(Tt)TM_{\mathcal{T}}$  gathers all quantum numbers of the three-body state. Since the three-body matrix elements depend on four Jacobi momenta, bra and ket states are organized into collective indices  $I = (pq\alpha)$  and  $I' = (p'q'\alpha')$  such that a matrixlike object  $M_{II'}$  is obtained from the initial  $M_{pqp'q'}^{\alpha\alpha'}$ .

For the partial-wave decomposition, angular-momentum eigenstates are obtained by coupling angular momenta of the first two particles to a two-body subsystem with quantum numbers  $L, S, J$ , which are subsequently coupled with the angular momenta of the third particle to obtain the three-body quantum numbers  $\mathcal{J}$  and  $\mathcal{T}$ . We emphasize that by working in a symmetry-adapted basis, we maintain rotational invariance and parity/isospin conservation in the factorization, i.e.,  $[\tilde{V}_{3N}, \mathcal{J}^2] = [\tilde{V}_{3N}, \mathcal{J}_z] = [\tilde{V}_{3N}, \Pi] = [\tilde{V}_{3N}, \mathcal{T}^2] = [\tilde{V}_{3N}, \mathcal{T}_z] = 0$ . We note that a basis transformation mediated by a unitary matrix  $U$  can be very efficiently performed starting from an initial SVD format, since the matrix multiplication  $\tilde{V}_{3N} \equiv U^\dagger V_{3N} U$  can be executed by operating only on the (thin)  $L$  and  $R^\dagger$  components of  $V_{3N}$ . This can

enable speedups in such transformations, e.g., for generating single-particle matrix elements used in medium-mass calculations.

In the following, the partial-wave 3N matrix elements from Eq. (3) are taken as input for an rSVD solver. For the discretization of the momentum mesh we use  $N_p = N_q = 15$  points for both Jacobi momenta. Intermediate two-body quantum numbers are included up to  $J_{\text{max}} = 8$ . Partial waves are characterized by their three-body quantum numbers  $\mathcal{J}^\Pi \mathcal{T}$ .

Figure 2 displays the singular values of chiral 3N interactions. Figure 2(a) shows the individual unregularized N<sup>2</sup>LO operator topologies in the triton channel, i.e.,  $\mathcal{J}^\Pi \mathcal{T} = \frac{1}{2}^+ \frac{1}{2}$ , with the corresponding low-energy constants (LECs) set to unity in their respective natural units (see Ref. [3]). We observe a clear difference between the set of long-range pion-exchange topologies  $\{c_1, c_3, c_4\}$  that have a much slower falloff compared to the set  $\{c_D, c_E\}$  that encode midrange and short-range contributions. Still all topologies exhibit a strong suppression at very low ranks ( $\lesssim 0.25\%$ ) followed by a transition to a declining plateau-like region. Even for the long-range topologies the size of the singular values is suppressed to less than  $s_i \approx 2 \times 10^{-3}$  for the smallest 99%. In particular in the case of the  $c_E$  term all singular values are smaller than  $10^{-15}$  except the largest one which is of the order ten.

In Fig. 2(b) we include nonlocal regulators  $f_{\Lambda_{3N}}(p, q) = \exp[-((p^2 + \frac{3}{4}q^2)/\Lambda_{3N})^4]$ , where  $\Lambda_{3N}$  denotes the three-body cutoff here set to  $\Lambda_{3N} = 2.0 \text{ fm}^{-1}$ . The regularized matrix elements induce a stronger suppression of the singular value spectrum for all operator topologies. Similar findings as for N<sup>2</sup>LO are found at subleading orders [Fig. 2(c) for N<sup>3</sup>LO]: short-range relativistic corrections are more strongly suppressed than the long-range multipion exchange topologies. In general the N<sup>3</sup>LO terms have larger leading singular values and slower falloff in most cases. Finally we show realistic

chiral 3N forces (obtained after multiplication with the corresponding LEC values) in Fig. 2(d) for the 3N part of the “1.8/2.0” interaction [12] with  $\Lambda_{3N} = 2.0 \text{ fm}^{-1}$  at  $N^2\text{LO}$  and in Fig. 2(e) for the 3N part of the “EMN450” interaction [62] with  $\Lambda_{3N} = 450 \text{ MeV}$  at  $N^3\text{LO}$ .

In general the regularization yields a stronger suppression of singular values, while this effect is more pronounced for smaller cutoff  $\Lambda_{3N}$ . Furthermore, a comparison with the individual operator topologies in Figs. 2(a) and 2(c) indicates that the singular spectrum is dictated by the dominating topology. The slow falloff of the  $N^3\text{LO}$  two-pion-exchange contributions yields a slower suppression of singular values in the case of the “EMN450” interaction. For the full interactions we additionally investigate different partial-wave channels by varying angular momentum, parity, and isospin. We note that the matrix dimensions among partial-wave channels differ significantly ( $N = 7650$  for  $\mathcal{J}^{\pi}\mathcal{T} = \frac{1}{2}^{+}\frac{3}{2}$  up to  $N = 40050$  for  $\mathcal{J}^{\pi}\mathcal{T} = \frac{5}{2}^{+}\frac{1}{2}$ ). As a general trend, higher partial-wave channels with larger  $\mathcal{J}$  values show a slower falloff while their largest singular value is significantly smaller compared to, e.g., the triton channel. To gauge the low-rank character of higher partial-wave channels we later explore many-body calculations.

#### IV. TRITON CALCULATIONS

A first benchmark for low-rank interactions is provided by the solution of the three-body problem for the ground-state energy and point-proton radius of the triton, using a Faddeev code in partial-wave-decomposed form [63]. Figure 3 provides an overview of the relative error on the ground-state energy (top), expectation value of the 3N force (middle), and point-proton radius (bottom) as a function of decomposition rank for the “1.8/2.0” and “EMN450” interactions. Similar to Fig. 2 we study the impact on the final observables by keeping up to 1% of the leading singular values in the decomposition. In the Faddeev calculation, we incorporate the full-rank NN potential since we want to study the sensitivity to the low-rank properties of the 3N force. Since both interactions have been fitted to the triton binding energy, our full-rank calculations reproduce the experimental value of  $E_{\text{gs}}(^3\text{H})$ . However, the individual size of the 3N contribution is different among the interactions used, with  $\langle V_{3N} \rangle_{1.8/2.0} = 0.19 \text{ MeV}$  and  $\langle V_{3N} \rangle_{\text{EMN450}} = 0.67 \text{ MeV}$ , respectively. Consequently, we expect higher sensitivity in the case of the “EMN450” interaction in the following.

At low ranks ( $\leq 0.5\%$ ), the “EMN450” interaction yields consistently larger errors for all observables. This is in agreement with the slower falloff in the triton channel as observed in Fig. 2. Still, in all cases keeping the leading 1% of singular values yields an excellent reproduction of ground-state properties with absolute differences of  $10^{-4} \text{ MeV (fm)}$  for the binding energy (point-proton radius). In general the point-proton radius is less sensitive to the decomposition of the 3N forces since the 3N contribution is approximately 0.7% (6.4%) for the “1.8/2.0” (“EMN450”) interaction. Few-body calculations thus allow for data compression of more than two orders of magnitude without significant loss in accuracy.

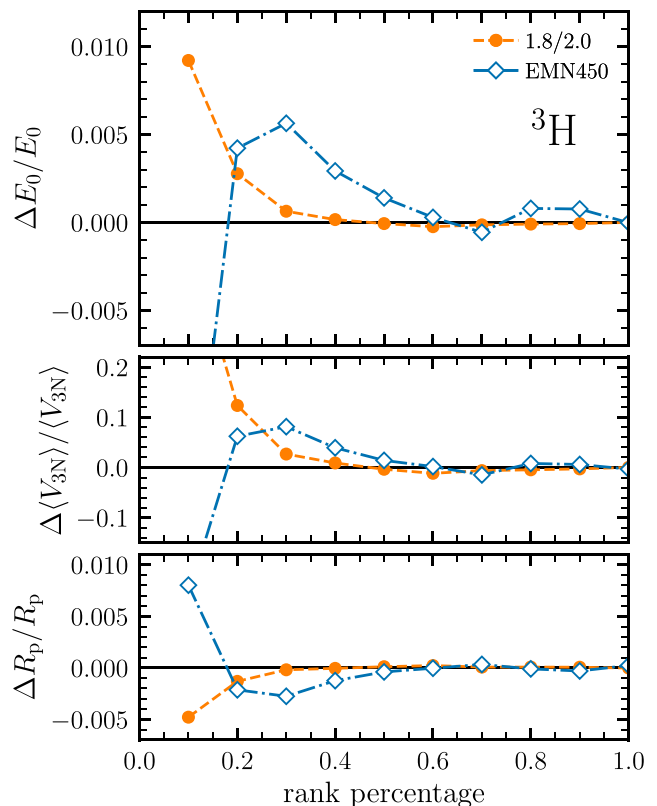


FIG. 3. Relative error on the ground-state energy (top), expectation value of the 3N force (middle), and point-proton radius (bottom) for the triton as a function of SVD rank. The NN interaction is not SVD-approximated. Results are shown for the “1.8/2.0” and “EMN450” interactions.

#### V. MEDIUM-MASS NUCLEI

To test the performance of low-rank 3N interactions for nuclei, we transform the matrix elements to a bound-state harmonic-oscillator basis. Subsequently, we solve the Hartree-Fock equations with NN+3N interactions, thus obtaining an energetically optimized reference state. Using normal ordering, the resulting zero-, one-, and two-body parts of the intrinsic Hamiltonian define the starting point for an IMSRG calculation that nonperturbatively accounts for particle-hole correlations [25]. We employ the IMSRG(2) approximation, the current standard in IMSRG calculations, where operators are truncated at the normal-ordered two-body level. Other observables are evaluated by a final transformation of the associated operators using the Magnus approach [64]. In addition, second-order MBPT results ( $E_{\text{MP2}}$ ) are shown as a simpler estimate for the correlation energy. Calculations are performed using the publicly available IMSRG solver by Stroberg [65].

As a benchmark we compare ground-state energies and charge radii of selected closed-shell nuclei ranging from  $^{16}\text{O}$  to  $^{132}\text{Sn}$  with the developed low-rank 3N interactions. All calculations employ 3N matrix elements with  $E_{3\text{max}} = 24$  using a storage format optimized for the normal-ordered two-body approximation [5]. Matrix element files are generated with the NUHAMIL code [66].

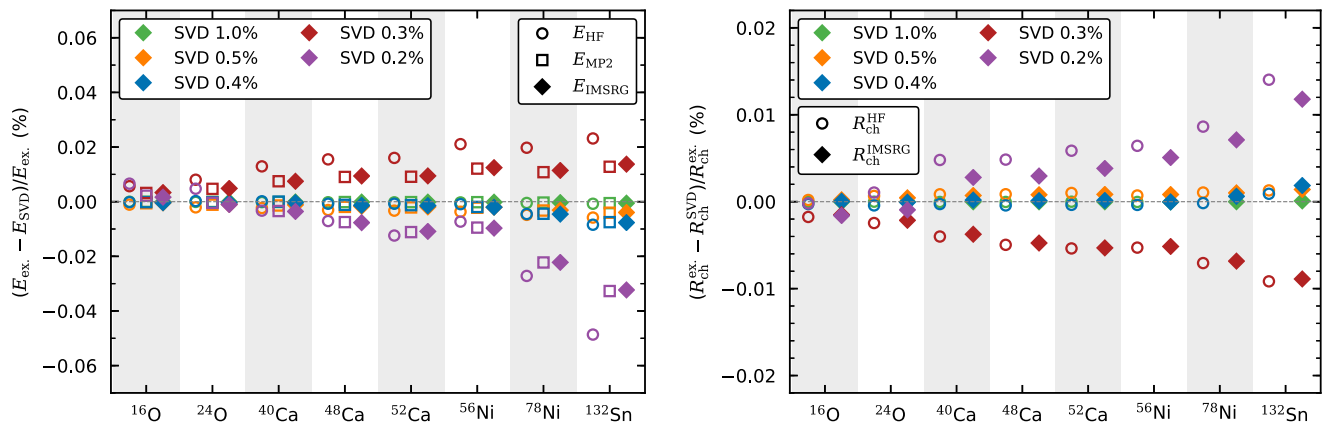


FIG. 4. Ground-state energies and charge radii at different many-body levels as a function of  $R_{\text{SVD}}^{\%}$  for selected closed-shell nuclei using the “1.8/2.0” interaction. Calculations were performed in a large space with  $e_{\text{max}} = 14$ ,  $E_{3\text{max}} = 24$ ,  $\hbar\Omega = 16$  MeV.

Figure 4 shows the relative error on the ground-state energy keeping  $R_{\text{SVD}}^{\%} = 0.2, 0.3, 0.4, 0.5, 1.0$  of the leading singular values. We observe in all cases that the impact of the SVD error is slightly larger at HF level compared to the MP2 and IMSRG(2) results. For both ground-state energies and charge radii there is a systematic decrease of the relative error as a function of  $R_{\text{SVD}}^{\%}$ , although the dependence is nonmonotonic. Still, in all cases the relative error is well below 0.1%. Moreover, a systematic increase of the relative error as a function of mass number is evident. Since this trend is already present at the HF level, we attribute the increase in error to the enlarged hole space in heavier systems and, thus, an enhanced accumulation of errors from individual matrix elements. The error on the correlation energy itself, both at the MP2 and IMSRG(2) level, does not increase in heavier systems. Even for the heaviest systems, the SVD error is only at the few hundred keV level.

## VI. SUMMARY AND OUTLOOK

We explored low-rank matrix decompositions of three-body operators using a randomized SVD algorithm. This method is applied to chiral 3N interactions that are key in nuclear *ab initio* calculations. We have clearly identified low-rank patterns in their momentum-space representation that enable efficient data compression. In our few- and many-body benchmarks low-rank three-body interactions provide an excellent approximation for nuclear ground-state observables, thus paving the way for new efficient data representations of large many-body operators. The memory savings that can be anticipated from our findings exceed a factor of  $C = 100$

at negligible approximation error on few- and many-body observables.

While the decomposition of many-body operators constitutes a natural first step, scaling benefits in actual applications require the reformulation of the many-body solver in terms of the decomposition factors themselves. The design of a factorized Faddeev solver is a natural starting point to increase performance in few-body applications. The transfer to the many-body sector constitutes a nontrivial open step that requires method-specific adaptations to provide computational gains. Factorization techniques define an innovative way of approaching new frontiers in nuclear physics [24,28]. Our findings clearly motivate the transfer to other domains of many-body research; whenever low-rank properties of operators can be identified, factorization approaches may induce great scaling advantages. In that context the rSVD serves as a robust tool to find such patterns.

## ACKNOWLEDGMENTS

This work was supported in part by the European Research Council (ERC) under the European Union’s Horizon 2020 research and innovation programme (Grant Agreement No. 101020842), the Deutsche Forschungsgemeinschaft (DFG, German Research Foundation)–Projektnummer 279384907 – SFB 1245, the Helmholtz Forschungsakademie Hessen für FAIR (HFHF) and by the BMBF Contract No. 05P21RDFNB. The authors gratefully acknowledge the Gauss Centre for Supercomputing e.V. [67] for funding this project by providing computing time through the John von Neumann Institute for Computing (NIC) on the GCS Supercomputer JUWELS at Jülich Supercomputing Centre (JSC).

- [1] K. Hebeler, J. D. Holt, J. Menéndez, and A. Schwenk, Nuclear forces and their impact on neutron-rich nuclei and neutron-rich matter, *Annu. Rev. Nucl. Part. Sci.* **65**, 457 (2015).
- [2] H. Hergert, A guided tour of *ab initio* nuclear many-body theory, *Front. Phys.* **8**, 379 (2020).
- [3] K. Hebeler, Three-nucleon forces: Implementation and applications to atomic nuclei and dense matter, *Phys. Rep.* **890**, 1 (2021).

- [4] T. D. Morris, J. Simonis, S. R. Stroberg, C. Stumpf, G. Hagen, J. D. Holt, G. R. Jansen, T. Papenbrock, R. Roth, and A. Schwenk, Structure of the lightest tin isotopes, *Phys. Rev. Lett.* **120**, 152503 (2018).
- [5] T. Miyagi, S. R. Stroberg, P. Navrátil, K. Hebeler, and J. D. Holt, Converged *ab initio* calculations of heavy nuclei, *Phys. Rev. C* **105**, 014302 (2022).

- [6] P. Arthuis, C. Barbieri, M. Vorabbi, and P. Finelli, *Ab initio* computation of charge densities for Sn and Xe isotopes, *Phys. Rev. Lett.* **125**, 182501 (2020).
- [7] B. Hu, W. Jiang, T. Miyagi, Z. H. Sun, A. Ekström, C. Forssén, G. Hagen, J. D. Holt, T. Papenbrock, S. R. Stroberg, and I. Vernon, *Ab initio* predictions link the neutron skin of  $^{208}\text{Pb}$  to nuclear forces, *Nature Phys.* **18**, 1196 (2022).
- [8] K. Hebeler, V. Durant, J. Hoppe, M. Heinz, A. Schwenk, J. Simonis, and A. Tichai, Normal ordering of three-nucleon interactions for *ab initio* calculations of heavy nuclei, *Phys. Rev. C* **107**, 024310 (2023).
- [9] A. Tichai, P. Demol, and T. Duguet, Towards heavy-mass *ab initio* nuclear structure: Open-shell Ca, Ni and Sn isotopes from Bogoliubov coupled-cluster theory, *Phys. Lett. B* **851**, 138571 (2024).
- [10] D. R. Entem, R. Machleidt, and Y. Nosyk, Nucleon-nucleon scattering up to  $N^5\text{LO}$  in chiral effective field theory, *Front. Phys.* **8**, 57 (2020).
- [11] E. Epelbaum, H. Krebs, and P. Reinert, High-precision nuclear forces from chiral EFT: State-of-the-art, challenges, and outlook, *Front. Phys.* **8**, 98 (2020).
- [12] K. Hebeler, S. K. Bogner, R. J. Furnstahl, A. Nogga, and A. Schwenk, Improved nuclear matter calculations from chiral low-momentum interactions, *Phys. Rev. C* **83**, 031301(R) (2011).
- [13] W. G. Jiang, A. Ekström, C. Forssén, G. Hagen, G. R. Jansen, and T. Papenbrock, Accurate bulk properties of nuclei from  $A = 2$  to  $\infty$  from potentials with  $\Delta$  isobars, *Phys. Rev. C* **102**, 054301 (2020).
- [14] J. D. Holt, J. Menéndez, J. Simonis, and A. Schwenk, Three-nucleon forces and spectroscopy of neutron-rich calcium isotopes, *Phys. Rev. C* **90**, 024312 (2014).
- [15] A. Tichai, J. Langhammer, S. Binder, and R. Roth, Hartree-Fock many-body perturbation theory for nuclear ground-states, *Phys. Lett. B* **756**, 283 (2016).
- [16] A. Tichai, P. Arthuis, T. Duguet, H. Hergert, V. Somà, and R. Roth, Bogoliubov many-body perturbation theory for open-shell nuclei, *Phys. Lett. B* **786**, 195 (2018).
- [17] A. Tichai, R. Roth, and T. Duguet, Many-body perturbation theories for finite nuclei, *Front. Phys.* **8**, 164 (2020).
- [18] W. H. Dickhoff and C. Barbieri, Self-consistent Green's function method for nuclei and nuclear matter, *Prog. Part. Nucl. Phys.* **52**, 377 (2004).
- [19] V. Somà, A. Cipollone, C. Barbieri, P. Navrátil, and T. Duguet, Chiral two- and three-nucleon forces along medium-mass isotope chains, *Phys. Rev. C* **89**, 061301(R) (2014).
- [20] V. Somà, P. Navrátil, F. Raimondi, C. Barbieri, and T. Duguet, Novel chiral Hamiltonian and observables in light and medium-mass nuclei, *Phys. Rev. C* **101**, 014318 (2020).
- [21] C. Barbieri, T. Duguet, and V. Somà, Gorkov algebraic diagrammatic construction formalism at third order, *Phys. Rev. C* **105**, 044330 (2022).
- [22] G. Hagen, T. Papenbrock, M. Hjorth-Jensen, and D. J. Dean, Coupled-cluster computations of atomic nuclei, *Rep. Prog. Phys.* **77**, 096302 (2014).
- [23] S. Binder, J. Langhammer, A. Calci, and R. Roth, *Ab initio* path to heavy nuclei, *Phys. Lett. B* **736**, 119 (2014).
- [24] S. J. Novario, G. Hagen, G. R. Jansen, and T. Papenbrock, Charge radii of exotic neon and magnesium isotopes, *Phys. Rev. C* **102**, 051303(R) (2020).
- [25] H. Hergert, S. K. Bogner, T. D. Morris, A. Schwenk, and K. Tsukiyama, The in-medium similarity renormalization group: A novel *ab initio* method for nuclei, *Phys. Rep.* **621**, 165 (2016).
- [26] S. R. Stroberg, H. Hergert, S. K. Bogner, and J. D. Holt, Nonempirical interactions for the nuclear shell model: An update, *Annu. Rev. Nucl. Part. Sci.* **69**, 307 (2019).
- [27] S. R. Stroberg, J. D. Holt, A. Schwenk, and J. Simonis, *Ab Initio* limits of atomic nuclei, *Phys. Rev. Lett.* **126**, 022501 (2021).
- [28] M. Heinz, A. Tichai, J. Hoppe, K. Hebeler, and A. Schwenk, In-medium similarity renormalization group with three-body operators, *Phys. Rev. C* **103**, 044318 (2021).
- [29] B. R. Barrett, P. Navrátil, and J. P. Vary, *Ab initio* no core shell model, *Prog. Part. Nucl. Phys.* **69**, 131 (2013).
- [30] J. Carlson, S. Gandolfi, F. Pederiva, S. C. Pieper, R. Schiavilla, K. E. Schmidt, and R. B. Wiringa, Quantum Monte Carlo methods for nuclear physics, *Rev. Mod. Phys.* **87**, 1067 (2015).
- [31] M. Frosini, T. Duguet, J.-P. Ebran, and V. Somà, Multi-reference many-body perturbation theory for nuclei: I. Novel PGCM-PT formalism, *Eur. Phys. J. A* **58**, 62 (2022).
- [32] M. Frosini, T. Duguet, J.-P. Ebran, B. Bally, T. Mongelli, T. R. Rodríguez, R. Roth, and V. Somà, Multi-reference many-body perturbation theory for nuclei: II. *Ab initio* study of neon isotopes via PGCM and IM-NCSM calculations, *Eur. Phys. J. A* **58**, 63 (2022).
- [33] M. Frosini, T. Duguet, J.-P. Ebran, B. Bally, H. Hergert, T. R. Rodríguez, R. Roth, J. M. Yao, and V. Somà, Multi-reference many-body perturbation theory for nuclei: III. *Ab initio* calculations at second order in PGCM-PT, *Eur. Phys. J. A* **58**, 64 (2022).
- [34] G. Hagen, S. J. Novario, Z. H. Sun, T. Papenbrock, G. R. Jansen, J. G. Lietz, T. Duguet, and A. Tichai, Angular-momentum projection in coupled-cluster theory: Structure of  $^{34}\text{Mg}$ , *Phys. Rev. C* **105**, 064311 (2022).
- [35] Q. Yuan, S. Q. Fan, B. S. Hu, J. G. Li, S. Zhang, S. M. Wang, Z. H. Sun, Y. Z. Ma, and F. R. Xu, Deformed in-medium similarity renormalization group, *Phys. Rev. C* **105**, L061303 (2022).
- [36] H.-W. Hammer, A. Nogga, and A. Schwenk, Three-body forces: From cold atoms to nuclei, *Rev. Mod. Phys.* **85**, 197 (2013).
- [37] T. G. Kolda and B. W. Bader, Tensor decompositions and applications, *SIAM Rev.* **51**, 455 (2009).
- [38] S. R. White, Density matrix formulation for quantum renormalization groups, *Phys. Rev. Lett.* **69**, 2863 (1992).
- [39] U. Schollwück, The density-matrix renormalization group in the age of matrix product states, *Ann. Phys. (NY)* **326**, 96 (2011).
- [40] A. Baiardi and M. Reiher, The density matrix renormalization group in chemistry and molecular physics: Recent developments and new challenges, *J. Chem. Phys.* **152**, 040903 (2020).
- [41] T. Papenbrock and D. J. Dean, Density matrix renormalization group and wavefunction factorization for nuclei, *J. Phys. G* **31**, S1377 (2005).
- [42] Ö. Legeza, L. Veis, A. Poves, and J. Dukelsky, Advanced density matrix renormalization group method for nuclear structure calculations, *Phys. Rev. C* **92**, 051303(R) (2015).
- [43] K. Fossez, J. Rotureau, N. Michel, and M. Płoszajczak, Can Tetraneutron be a Narrow Resonance? *Phys. Rev. Lett.* **119**, 032501 (2017).

- [44] A. Tichai, S. Knecht, A. T. Kruppa, Ö. Legeza, C. P. Moca, A. Schwenk, M. A. Werner, and G. Zarand, Combining the in-medium similarity renormalization group with the density matrix renormalization group: Shell structure and information entropy, *Phys. Lett. B* **845**, 138139 (2023).
- [45] A. Tichai, K. Kapás, T. Miyagi, M.A. Werner, Ö. Legeza, A. Schwenk, and G. Zarand, Spectroscopy of  $N = 50$  isotones with the valence-space density matrix renormalization group, *Phys. Lett. B* **855**, 138841 (2024).
- [46] T. Kinoshita, O. Hino, and R. J. Bartlett, Singular value decomposition approach for the approximate coupled-cluster method, *J. Chem. Phys.* **119**, 7756 (2003).
- [47] E. G. Hohenstein, S. I. L. Kokkila, R. M. Parrish, and T. J. Martínez, Quartic scaling second-order approximate coupled cluster singles and doubles via tensor hypercontraction: THC-CC2, *J. Chem. Phys.* **138**, 124111 (2013).
- [48] R. Schutski, J. Zhao, T. M. Henderson, and G. E. Scuseria, Tensor-structured coupled cluster theory. *J. Chem. Phys.* **147**, 184113 (2017).
- [49] R. M. Parrish, Y. Zhao, E. G. Hohenstein, and T. J. Martínez, Rank reduced coupled cluster theory. I. Ground state energies and wavefunctions, *J. Chem. Phys.* **150**, 164118 (2019).
- [50] M. Lesiuk, Quintic-scaling rank-reduced coupled cluster theory with single and double excitations, *J. Chem. Phys.* **156**, 064103 (2022).
- [51] U. Benedikt, A. A. Auer, M. Espig, and W. Hackbusch, Tensor decomposition in post-Hartree-Fock methods. I. Two-electron integrals and MP2, *J. Chem. Phys.* **134**, 054118 (2011).
- [52] U. Benedikt, K.-H. Böhm, and A. A. Auer, Tensor decomposition in post-Hartree-Fock methods. II. CCD implementation, *J. Chem. Phys.* **139**, 224101 (2013).
- [53] M. Motta, J. Shee, S. Zhang, and Garnet Kin-Lic Chan, Efficient *ab initio* auxiliary-field quantum Monte Carlo calculations in Gaussian bases via low-rank tensor decomposition, *J. Chem. Theory Comput.* **15**, 3510 (2019).
- [54] A. Tichai, P. Arthuis, K. Hebeler, M. Heinz, J. Hoppe, and A. Schwenk, Low-rank matrix decompositions for *ab initio* nuclear structure, *Phys. Lett. B* **821**, 136623 (2021).
- [55] B. Zhu, R. Wirth, and H. Hergert, Singular value decomposition and similarity renormalization group evolution of nuclear interactions, *Phys. Rev. C* **104**, 044002 (2021).
- [56] A. Tichai, P. Arthuis, K. Hebeler, M. Heinz, J. Hoppe, A. Schwenk, and L. Zurek, Least-square approach for singular value decompositions of scattering problems, *Phys. Rev. C* **106**, 024320 (2022).
- [57] A. Tichai, R. Schutski, G. E. Scuseria, and T. Duguet, Tensor-decomposition techniques for *ab initio* nuclear structure calculations: From chiral nuclear potentials to ground-state energies, *Phys. Rev. C* **99**, 034320 (2019).
- [58] A. Tichai, J. Ripoche, and T. Duguet, Pre-processing the nuclear many-body problem: Importance truncation versus tensor factorization techniques, *Eur. Phys. J. A* **55**, 90 (2019).
- [59] A. Zare, R. Wirth, C. A. Haselby, H. Hergert, and M. Iwen, Modewise Johnson-Lindenstrauss Embeddings for Nuclear Many-Body Theory, *Eur. Phys. J. A* **59**, 95 (2023).
- [60] N. Halko, P. G. Martinsson, and J. A. Tropp, Finding structure with randomness: Probabilistic algorithms for constructing approximate matrix decompositions, *SIAM Rev.* **53**, 217 (2011).
- [61] G. Guennebaud, B. Jacob *et al.*, Eigen v3 (2010), <https://gitlab.com/libeigen/eigen>.
- [62] C. Drischler, K. Hebeler, and A. Schwenk, Chiral Interactions up to next-to-next-to-next-to-leading order and nuclear saturation, *Phys. Rev. Lett.* **122**, 042501 (2019).
- [63] A. Stadler, W. Glöckle, and P. U. Sauer, Faddeev equations with three-nucleon force in momentum space, *Phys. Rev. C* **44**, 2319 (1991).
- [64] T. D. Morris, N. M. Parzuchowski, and S. K. Bogner, Magnus expansion and in-medium similarity renormalization group, *Phys. Rev. C* **92**, 034331 (2015).
- [65] S. R. Stroberg, ragnarstroberg/imsrg (2019), <https://github.com/ragnarstroberg/imsrg>.
- [66] T. Miyagi, NuHamil : A numerical code to generate nuclear two- and three-body matrix elements from chiral effective field theory, *Eur. Phys. J. A* **59**, 150 (2023).
- [67] [www.gauss-centre.eu](http://www.gauss-centre.eu)